Sheath structure and formation of dust voids in cylindrical plasma discharges

Zuquan Hu (胡祖权),[1] Yinhua Chen (陈银华),[1,*] Feng Huang (黄凤),[1] Gui-fen Shi (时桂芬),[1]
Jugao Zheng (郑聚高),[1] and M. Y. Yu (郁明阳)[2,3]
[1]*Key Laboratory of Basic Plasma Physics, Chinese Academy of Sciences, and Department of Modern Physics, University of Science and Technology of China (USTC), 230026 Hefei, China*
[2]*Institute for Fusion Theory and Simulation, Department of Physics, Zhejiang University, 310027 Hangzhou, China*
[3]*Institute für Theoretische Physik, Ruhr-Universität Bochum, D-44780 Bochum, Germany*
(Received 28 January 2010; published 4 May 2010)

Using a self-consistent two-dimensional fluid model the structure of the plasma sheath in a cylindrical system is investigated. The results show that there is a bumping potential in the central axis resulting in the larger outward directing ion drag force with respect to the opposite electric field force. And the process of the formation of dust voids is studied in the sheath by molecular-dynamics simulation.

DOI: 10.1103/PhysRevE.81.056401 PACS number(s): 52.27.Lw, 52.40.Kh, 52.65.Yy, 52.80.Pi

I. INTRODUCTION

In the past decade there has been much experimental and theoretical interest in the formation of dust voids in plasmas containing dust grains [1–21]. A dust void is a centimeter-sized region completely free of dust particles and it has a sharp boundary that oscillates at the dust-acoustic wave time scale of several hertz [1].

Samsonov and Goree [2,3] suggested that dust voids are formed because of balance of the ion drag and electrostatic forces on the dust grains. Morfill *et al.* [4] showed that the thermophoretic force on the grain can also play a role. Avinash *et al.* [16] proposed a time-dependent fluid model for the void formation process that is initiated by the ion drag force and saturated by ion-neutral collisions. Hu *et al.* [17] extended the model of Avinash *et al.* [16] by including the effect of ionization and found that the obtained void characteristics are consistent with that from the experiments [2,3,6–8]. Denysenko *et al.* [9–12] considered in more detail the electron kinetics and other kinetic effects in dusty plasmas and showed that balance of forces on the dusts can affect the spatial electron distribution, the plasma temperature, the discharge potential, as well as the plasma transport properties, which can in turn govern the dust dynamics. Huang *et al.* [6,7] found experimentally that voids in a dusty discharge can have domelike and shell-like structures, which together with even more exotic forms relevant to material structures have been obtained from molecular-dynamics (MD) simulations where the dust grains are trapped in different potentials [19–21]. In this paper, we consider the process of dust formation in more detail by first obtaining the sheath potential of the discharge plasma using a fluid model for the dust grains. The effects of the sheath electric field and ion drag force, as well as the experimental discharge configuration, are included [6,7,9–12]. The resulting electrostatic potential in the plasma sheath is then used to investigate the formation of dust voids by MD simulation. Our results agree qualitatively well with those of the experiments.

*yhchen@ustc.edu.cn

II. MODEL OF THE SHEATH

In the standard steady-state fluid model of a plasma sheath, the electrons are assumed to obey the Boltzmann density profile $n_e=n_{e0}\exp(e\Phi/T_e)$, where n_e, $-e$, and T_e are the electron density, charge, and temperature and n_{e0} is the electron density in the unperturbed plasma where the electrostatic potential Φ vanishes, that is, far from the discharge boundary. The ions are described by the continuity equation $\nabla\cdot(n_i\boldsymbol{u})=0$ and the momentum equation $m_i n_i(\boldsymbol{u}\cdot\nabla)\boldsymbol{u}=-en_i\nabla\Phi-\nabla(n_iT_i)-\nu m_i n_i\boldsymbol{u}$, where the last three terms are the electrostatic, pressure, and frictional forces on the ions, respectively. Here, $\boldsymbol{u}$ is the ion fluid velocity and $\nu=uN_n\sigma_c$ is the ion-neutral collision frequency, with N_n being the neutral gas number density, σ_c being the total collision cross section [24], and $u=|\boldsymbol{u}|$. The system is closed by the Poisson equation $\nabla^2\Phi=-4\pi e(n_i-n_e)$.

A schematic of the vertical cylindrical discharge with a disklike center electrode and a ringlike edge electrode at its bottom, as in the experiments of Huang *et al.* [6,7], is given in Fig. 1(a). The height L of the upper boundary is much larger than the sheath thickness, so that the upper part of the discharge plasma is quasineutral, $n_{e0}=n_{i0}=n_0$, and we can assume $\phi|_{z=L}=0$. An extrapolative inflow boundary condition is used to determine the inlet velocity u_0 of the ions on the upper discharge surface at $z=L$. That is, the ion inflow velocity is determined from the ion velocities at the interior nodes of the simulation grid: $u_0=2u_1-u_2$, where u_1 and u_2 are the first two nodes [22]. Because of symmetry, $\partial_r=0$ is assumed on the axis $r=0$, as well as at the boundary $r=R$ of the discharge. The voltage of the center electrode at the discharge bottom is kept constant at $\Phi|_{z=0}=V_0$. The potential of the outer bottom electrode, whose width is much larger than the electron Debye length, is obtained from the ion- and electron-flux balance conditions [23]. Similarly, the extrapolative outflow condition [22] is used to obtain the ion velocity at the inner surface of the outer bottom electrode, as well as the outer and upper surfaces of the center bottom electrode. The radial ion velocity u_r on the axis $r=0$ as well as on the discharge boundary $r=R$ is set to zero. Note that the conditions at the outer discharge boundary are not crucial since the radius and width of the outer electrode EE are

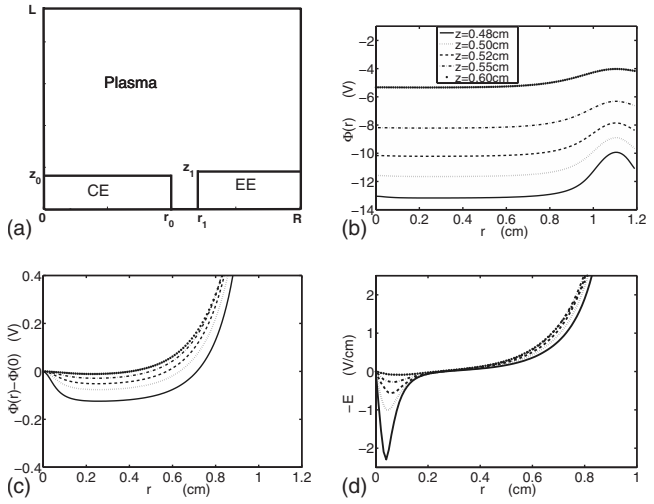

FIG. 1. (a) Sketch of the cylindrical discharge. Here, CE and EE denote center and edge electrodes, respectively, $r_0=1.0$ cm, $r_1=1.2$ cm, $R=2.0$ cm, $z_0=0.40$ cm, $z_1=0.45$ cm, and $L=2.4$ cm $(=60\lambda_d)$. (b) The potential at different heights in the sheath region. (c) The relative potential (with respect to that on the axis) in the sheath region. (d) The electric field in the sheath region. The legend in (b) also applies to (c) and (d).

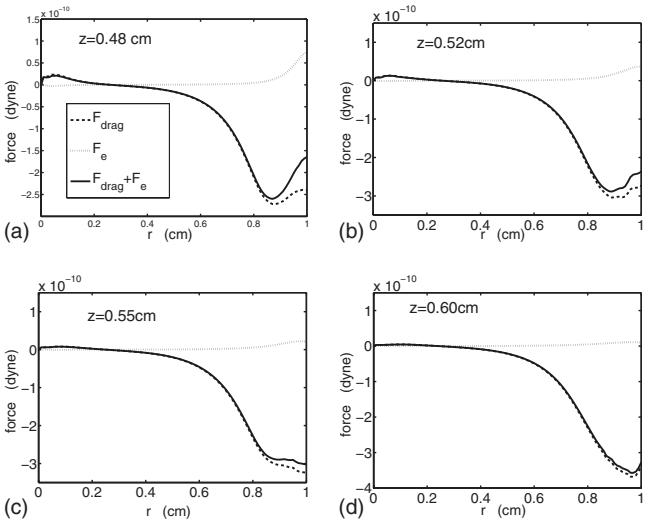

FIG. 2. The ion drag force, electric field force, and the total force acting on the test grain.

much larger than the Debye length, and the rarefied plasma above it is far from the region of interest, which is just above the center electrode CE. In fact, the self-consistent plasma region where the dust structures are found is determined mainly by the conditions on the axis, as well as the bottom boundary where the Boris outflow condition is applied.

Following the experimental conditions [6,7], we set the upper boundary of the discharge at $z=L=60\lambda_d=2.4$ cm, the radius of the center electrode (lower left in Fig. 1) at the bottom of the discharge at $r=r_0=1.0$ cm, the inner side of the outer electrode (lower right in Fig. 1) at $r=r_1=1.2$ cm, the radial boundary of the discharge at $r=R=2.0$ cm, and the heights of center and outer electrodes at $z_0=0.40$ cm and $z_1=0.45$ cm, respectively. We also consider a weakly ionized argon plasma. The electron and ion temperatures are 3.0 and 0.025 eV, respectively. The density of the plasma at the upper boundary is $n_0=1.0\times10^9$ cm^{-3} and the pressure of the neutral argon gas is 300 Pa. The voltage of the center electrode is −20 V and the outer electron is grounded. In the simulation, the space is normalized by the electron Debye length λ_{de}, which for the given parameters is 0.04 cm and much less than any of the characteristic lengths.

III. NUMERICAL RESULTS

We are interested in the sheath region near the electrodes, that is, the lower part of the discharge. Figure 1(b) shows the potential at different values of z. We see that the potential remains radially constant for each z until $r>0.8$, where a bump occurs because of the outer (ringlike) electrode at the bottom. On the other hand, careful inspection shows that there is a small potential dip in the region $0.1<r<0.7$ cm, as can be seen more clearly in Fig. 1(c) for $\phi(r)-\phi(0)$ versus r. The magnitude of the potential dip decreases as z increases. The corresponding electric field in this region is given in Fig. 1(d), where one can see a rather large peak in the sheath (smaller z) region for $r<0.2$ cm near the axis. The field is radially outward and it decreases with the height, in contrast to that in the region $0.4<r<1.0$ cm.

Figure 2 shows the ion drag force $F_{\rm drag}$, the electric force $F_e=Q_dE$, and their sum $F_{\rm drag}+F_e$, acting on a dust grain of radius $r_d=0.4$ μm in the sheath at different heights. The local dust charge $Q_d\sim\mathcal{O}(-500e)$ is obtained from the standard orbit-motion-limited theory and the ion drag force is calculated including Debye shielding, finite grain size, and local grain-charging effects [11–16,25–28]. We see in Fig. 2(a) that for $r\lesssim0.3$ cm the total force $F_{\rm drag}+F_e$ is directed radially outward, that is, in the same direction as $F_{\rm drag}$ since $|F_{\rm drag}|>|F_e|$. In the region $0.3\lesssim r\lesssim0.8$ cm, one can see that as r increases, $F_{\rm drag}$ increases faster than F_e, so that eventually the total force $F_{\rm drag}+F_e$ becomes directed inward as well as increases with r, as shown in Figs. 2(c) and 2(d). The overall properties of the curves in the latter figures as well as in Fig. 2(b) are similar to that of Fig. 2(a) for $r<0.8$ cm, but one can see that for $r\lesssim3.0$ cm the magnitudes of the forces diminish with increasing height. Furthermore, at $r\simeq0.26$ cm the total force $F_{\rm drag}+F_e=0$ remains almost unchanged. The local force-balance results here determine the location and properties of the dust void in the discharge, as shall be confirmed by MD simulation of the evolution of dust voids in the next section.

IV. MD SIMULATION OF VOID FORMATION

The equation of motion of the dust grain j is

$$m_{dj}d\boldsymbol{v}_{dj}/dt=-Q_j\nabla V_j+\boldsymbol{F}_{{\rm drag}j}+\boldsymbol{F}_{Ej}+m_{dj}\boldsymbol{g}, \qquad (1)$$

where m_{dj}, $\boldsymbol{v}_{dj}$, and Q_j are the mass, velocity, and charge of the dust grain j; $\boldsymbol{g}$ is the gravitational acceleration; $V_j=\Sigma_{k=1,k\neq j}^{k=N}Q_jQ_k\exp(-r_{jk}/\lambda_{de})/r_{jk}$ is the sum of the interaction potentials of the grain j with the other (k) grains; N is the total number of grains; $\boldsymbol{r}_{jk}=|\boldsymbol{r}_j-\boldsymbol{r}_k|$; and $\boldsymbol{F}_{{\rm drag}j}=m_in_i\gamma_{jk}\boldsymbol{u}_i$

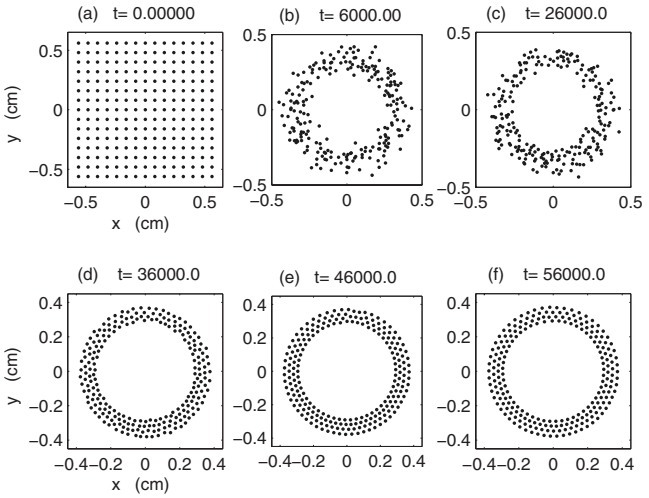

FIG. 3. Process of void formation at $z=0.48$ cm in the sheath, from MD simulation.

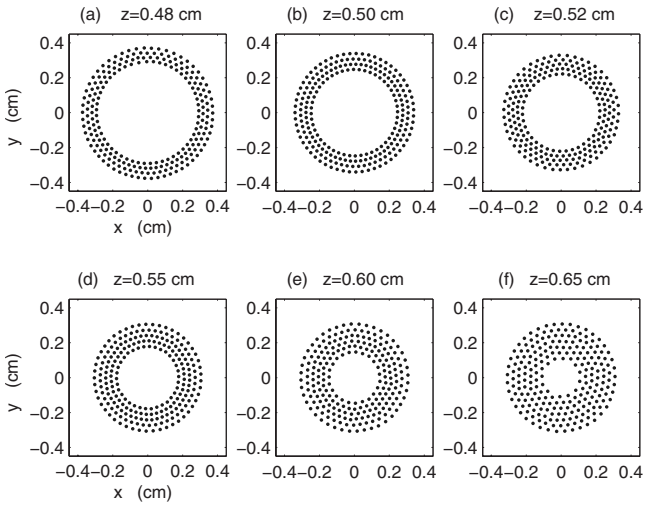

FIG. 4. Voids at different heights in the sheath, from MD simulation.

[27,28] and $\boldsymbol{F}_E=Q_j\boldsymbol{E}_j$ are the ion drag and electric forces acting on the dust grain j, respectively. In the simulation, the dust-grain radius is $r_d=0.4$ μm and the dust density is $n_d=10^3-10^4$ cm^{-3}. The time is normalized by the inverse dust plasma frequency $\omega_{pd}^{-1}\sim 0.05$ s.

At different heights in the sheath, the z components of the ion drag, electric, and the (screened) Coulomb intergrain forces acting on the dust grain j have the following ordering: $F_{Ejz}\sim 10^{-9}$ dyne, $F_{\mathrm{drag}jz}\sim 10^{-11}$ dyne, and $F_{jkz}\sim 10^{-12}$ dyne, or $F_{Ejz}\gg F_{\mathrm{drag}jz}\gg F_{kjz}$. Thus, in the vertical direction the electric and gravitational forces are much larger than the other forces, so that the positions of the dust grains in the z direction are determined by the local balance of these forces on a time scale much shorter than that in the horizontal direction. Accordingly, the dust dynamics in the horizontal direction can be separated from that in the vertical direction and the problem can be considered as two dimensional (2D), as has been noticed and invoked in the existing theoretical and experimental studies of dusty plasmas [1–8,13–21,29].

In order to investigate the dust-void formation process, the dust system is slowly heated from $T_d=0.001$ to 0.01 eV. Annealing at a rate of $\sim 3.33\times 10^{-9}$ eV/step is then applied until the system reaches a low-temperature ($\sim 10^{-8}$ eV) state and a stable dust void emerges [19–21].

A typical scenario of void formation in the sheath is shown in Fig. 3. The MD simulation is initiated with a uniform spatial distribution and a random velocity distribution of the dust grains. After the system is heated to 0.01 eV at $t=6000$, as shown in Fig. 3(b), the spatial grain distribution becomes disordered. Because of the intergrain repelling force and the large ion drag force at the center and the opposite ion drag force for $r>0.3$ cm, the grains become confined in the region $r\sim 0.4$ cm. As the grains are cooled, their distribution becomes more orderly and a void begins to form. At $t=56\,000$, a highly symmetrical (circular) void with a sharp boundary appears. Its center is completely free of dust grains.

Figure 4 shows the final states of the dust grains at different heights. We can see that the diameter of the circular void region decreases with the increase in the height in the sheath. For example, the void diameter at $z=0.48$ cm is about 0.6 cm, but it becomes 0.20 cm at $z=0.65$ cm. Such a behavior is also observed in the experiments [6,7]. Moreover, the voids at the heights $z=0.48-0.65$ cm have sharp boundaries and the grains in the dusty region are distributed in a latticelike manner, which has also been observed in the experiments [2,4,6,7].

The MD simulation results shown in Fig. 4 for the formation of the void can be explained in terms of the local force balance. As mentioned, in the vicinity of the discharge axis the outward ion drag force on a dust grain is larger than the inward electric force; the grains in this region will be pushed out and a void will be formed. The ion drag force on the dust grain decreases with its height in the sheath in the center region $r<0.3$ cm. As a result, the grains are less pushed out and the diameter of the void becomes smaller. On the other hand, for larger r values the force balance at different heights remains almost the same, so that the positions of the outer boundary of the dusty regions do not change much with the sheath height. The lattice structuring of the grains in the dusty region can be attributed to the intergrain force and the high value of the Coulomb coupling parameter ($\Gamma=n_d^{1/3}Q^2/T_d$) of the dusts [30]. Our 2D MD simulation is valid for the low dust density system considered since, as discussed, the force-balance time in the vertical direction is much shorter than that in the horizontal direction. For higher dust densities, say $n_d\geq 10^7$ cm^{-3}, three-dimensional effects may have to be included because of the stronger interaction among the dusts.

If we reverse the annealing process after a void is formed, defects and asymmetry can appear in the latticelike dust structure enclosing the void. Figure 5 shows such an asymmetric structure at $z=0.50$ cm when the system corresponding to Fig. 4(b) is gradually heated from 10^{-8} to 0.10 eV. Asymmetry can appear because the ion drag force on the grains is velocity dependent, so that the initial azimuthal symmetry in the dust momentum-vector distribution is not strictly preserved during the annealing and reverse annealing. As a result, for long simulation runs, there can be a

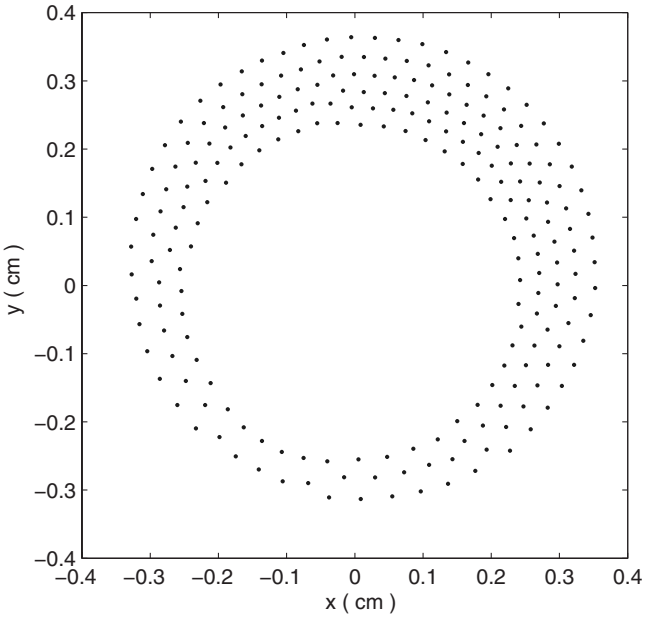

FIG. 5. A noncircular void at $z=0.50$ cm, from MD simulation at higher dust temperature.

gradual shift of the center of mass of the system together with loss of its symmetry. Asymmetric structures have also been observed in the experiments [6,7], but they are probably due to imperfections of the walls.

In the analysis and simulations presented here, the voltage of the center electrode is kept constant at −20 V. We have also investigated a wide range of other voltage values and found that the results are physically similar, in particular the profile of the electric potential near the center and near the outer boundary of the cylindrical discharge, as well as the variation of the location of the voids with the grain size. Thus, the formation process and properties of the dust-void structures are rather robust.

V. SUMMARY

In this paper we first obtained the potential of the plasma sheath by solving self-consistently the fluid model for a dusty plasma similar to that investigated experimentally by Huang *et al.* [6,7]. It is shown that the presence of a radial structure of the electric potential in the sheath region favors void formation because of the local balance of forces on the dust grains. MD simulation of the void formation process is used to verify the predicted location and properties of the dust voids. The latter also qualitatively agree with that observed in the dust-void experiments [6,7].

ACKNOWLEDGMENTS

This work was supported by the National Natural Science Foundation of China (Contracts No. 40831062, No. 10775134, and No. 10835003), the Chinese Academy of Sciences (Contract No. kjcx2-yw-n28), the National Basic Research Program of China (Contracts No. 2008CB717800 and No. 2008CB717806), the National Hi-Tech Inertial Confinement Fusion Committee of China, and the Ministry of Science and Technology of China Special Project for ITER (Contracts No. 2009GB105001 and No. 2009GB105005).

[1] G. Praburam and J. Goree, Phys. Plasmas **3**, 1212 (1996).
[2] D. Samsonov and J. Goree, Phys. Rev. E **59**, 1047 (1999).
[3] D. Samsonov and J. Goree, IEEE Trans. Plasma Sci. **27**, 76 (1999).
[4] G. E. Morfill, H. M. Thomas, U. Konopka, H. Rothermel, M. Zuzic, A. Ivlev, and J. Goree, Phys. Rev. Lett. **83**, 1598 (1999).
[5] R. P. Dahiya, G. V. Paeva, W. W. Stoffels, E. Stoffels, G. M. W. Kroesen, K. Avinash, and A. Bhattacharjee, Phys. Rev. Lett. **89**, 125001 (2002).
[6] F. Huang, M. F. Ye, L. Wang, and N. Jiang, Chin. Phys. Lett. **21**, 121 (2004).
[7] F. Huang, M. F. Ye, and L. Wang, Chin. Sci. Bull. **49**, 24 (2004).
[8] M. Mikikian and L. Boufendi, Phys. Plasmas **11**, 3733 (2004).
[9] I. Denysenko, M. Y. Yu, K. Ostrikov, N. A. Azarenkov, and L. Stenflo, Phys. Plasmas **11**, 4959 (2004).
[10] I. Denysenko, M. Y. Yu, L. Stenflo, and N. A. Azarenkov, Phys. Plasmas **12**, 042102 (2005).
[11] I. Denysenko, K. Ostrikov, M. Y. Yu, and N. A. Azarenkov, Phys. Rev. E **74**, 036402 (2006).
[12] I. Denysenko, M. Y. Yu, and N. A. Azarenkov, Phys. Plasmas **13**, 013505 (2006).
[13] J. Goree, G. E. Morfill, V. N. Tsytovich, and S. V. Vladimirov, Phys. Rev. E **59**, 7055 (1999).
[14] V. N. Tsytovich, S. V. Vladimirov, G. E. Morfill, and J. Goree, Phys. Rev. E **63**, 056609 (2001).
[15] X. Wang, A. Bhattacharjee, S. K. Gou, and J. Goree, Phys. Plasmas **8**, 5018 (2001).
[16] K. Avinash, A. Bhattacharjee, and S. Hu, Phys. Rev. Lett. **90**, 075001 (2003).
[17] Zuquan Hu, Yinhua Chen, Xiang Zheng, Feng Huang, Gei-fen Shi, and M. Y. Yu, Phys. Plasmas **16**, 063707 (2009).
[18] M. R. Akdim and W. J. Goedheer, Phys. Rev. E **65**, 015401(R) (2001); **67**, 066407 (2003).
[19] Y. H. Liu, Z. Y. Chen, F. Huang, M. Y. Yu, L. Wang, and A. Bogerts, Phys. Plasmas **13**, 052110 (2006).
[20] Y. H. Liu, Z. Y. Chen, M. Y. Yu, and A. Bogaerts, Phys. Rev. E **74**, 056401 (2006).
[21] Y. H. Liu, L. Y. Chew, and M. Y. Yu, Phys. Rev. E **78**, 066405 (2008).
[22] J. P. Boris, A. M. Landsberg, E. S. Oran, and J. H. Gardner, Naval Research Laboratory Memorandum Report No. 6410-93-7192, 1993 (unpublished).
[23] P. K. Shukla and A. A. Mamun, *Introduction to Dusty Plasma Physics* (Institute of Physics, Bristol, 2002).
[24] D. Kim and D. J. Economou, IEEE Trans. Plasma Sci. **30**,

2048 (2002).
[25] V. E. Fortov, A. G. Khrapak, S. A. Khrapak, V. I. Molotkov, and O. F. Petrov, Usp. Fiz. Nauk **174**, 495 (2004) [Phys. Usp. **47**, 447 (2004)].
[26] E. C. Whipple, Rep. Prog. Phys. **44**, 1197 (1981).
[27] S. A. Khrapak, A. V. Ivlev, G. E. Morfill, and H. M. Thomas, Phys. Rev. E **66**, 046414 (2002).
[28] S. A. Khrapak, A. V. Ivlev, S. K. Zhdanov, and G. E. Morfill, Phys. Plasmas **12**, 042308 (2005).
[29] K. N. Ostrikov, M. Y. Yu, and L. Stenflo, Phys. Rev. E **61**, 782 (2000).
[30] H. Ikezi, Phys. Fluids **29**, 1764 (1986).